

# Quantum Mechanical Description of Raman Scattering from Molecules in Plasmonic Cavities

Mikolaj K. Schmidt,<sup>\*,†,‡</sup> Ruben Esteban,<sup>‡</sup> Alejandro González-Tudela,<sup>¶</sup> Geza Giedke,<sup>‡,§</sup> and Javier Aizpurua<sup>\*,†,‡</sup>

<sup>†</sup>Materials Physics Center CSIC-UPV/EHU, Paseo Manuel de Lardizabal 5, 20018 Donostia-San Sebastián, Spain

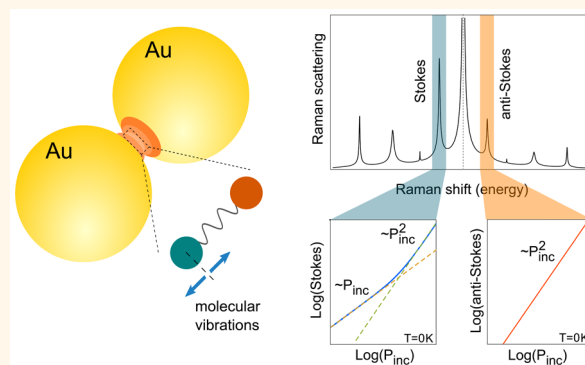
<sup>‡</sup>Donostia International Physics Center DIPC, Paseo Manuel de Lardizabal 4, 20018 Donostia-San Sebastián, Spain

<sup>¶</sup>Max-Planck-Institut für Quantenoptik, Hans-Kopfermann-Strauße 1, 85748 Garching, Germany

<sup>§</sup>IKERBASQUE, Basque Foundation for Science, Maria Diaz de Haro 3, 48013 Bilbao, Spain

## Supporting Information

**ABSTRACT:** Plasmon-enhanced Raman scattering can push single-molecule vibrational spectroscopy beyond a regime addressable by classical electrodynamics. We employ a quantum electrodynamics (QED) description of the coherent interaction of plasmons and molecular vibrations that reveal the emergence of nonlinearities in the inelastic response of the system. For realistic situations, we predict the onset of *phonon-stimulated Raman scattering* and a counterintuitive dependence of the anti-Stokes emission on the frequency of excitation. We further show that this QED framework opens a venue to analyze the correlations of photons emitted from a plasmonic cavity.



**KEYWORDS:** quantum electrodynamics, Raman scattering, SERS, Stokes emission, plasmonics, quantum nanooptics

Surface enhanced Raman scattering (SERS) is a spectroscopic technique in which the inelastic scattering from a molecule is increased by placing it in a *hotspot* of a plasmonic cavity, where the electric fields associated with the incident and the scattered photons are strongly enhanced (see the schematic in Figure 1a).<sup>1</sup> The difference between the energy of those two photons provides a *fingerprint* of the molecule, that is, detailed chemical information about its vibrational structure. Since the initial observation of Raman scattering from single molecules,<sup>2,3</sup> the use of a variety of plasmonic structures that act as effective optical nanoantennas over the last decades has allowed a tremendous advance of this molecular spectroscopy.<sup>4</sup> Metallic particles such as nano-shells,<sup>5,6</sup> nanorings,<sup>7</sup> nanorods,<sup>8</sup> nanowires,<sup>9</sup> or nano stars,<sup>10</sup> as well as plasmonic nanogap structures formed in particle dimers,<sup>11–13</sup> nanoparticle-on-a-mirror morphologies,<sup>14–17</sup> or nanoclusters<sup>18</sup> are among the variety of structures that offer huge and controllable enhancements of the field intensity in their hotspots, boosting the inherently weak Raman scattering intensity,<sup>1,19</sup> and ultimately enabling the chemical identification and imaging of particular vibrational modes of a molecule with subnanometer resolution.<sup>20</sup> These results suggest that some experiments might have reached the regime where the

quantum-mechanical nature of both the molecular vibrations and the plasmonic cavity emerges<sup>21</sup> and call for an adequate theoretical description that goes beyond the classical treatment of the electric fields produced in plasmonic cavities.<sup>1,22,23</sup>

In this work, we address the underlying quantum-mechanical nature of Raman scattering processes by quantizing as bosonic excitations both the vibrations of the molecule and the electromagnetic field of a plasmonic cavity. The description of the vibrations through bosonic operators can be justified by considering the harmonic approximation to the energy landscape of the molecule along a generalized atomic coordinate (Figure 1b), such as the length of a molecular bond, for example, C=O.<sup>21,22</sup> These vibrations interact with the cavity photons through a nonlinear Hamiltonian, reminiscent of that found in optomechanical systems.<sup>24</sup> In this description, the large enhancement of the Raman scattering from a molecule in the plasmonic cavity occurs thanks to the significant shrinking of the effective mode volume of a single photon. On the other hand, such plasmonic systems experience

Received: April 12, 2016

Accepted: May 20, 2016

Published: May 20, 2016

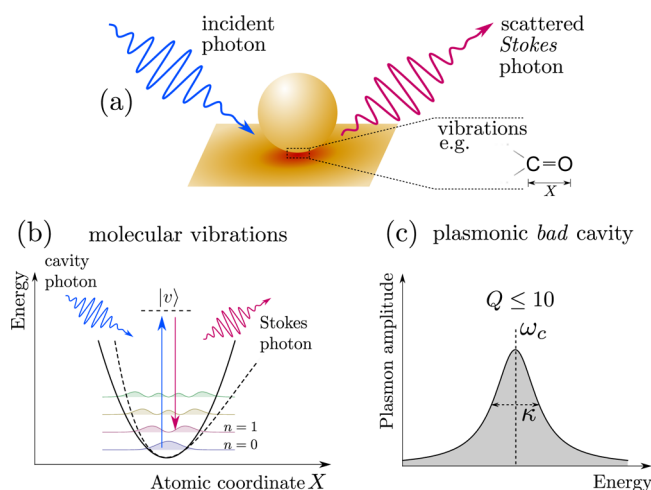


**Figure 1.** (a) Schematic of a setup for observing the Raman scattering from a molecule placed in a plasmonic cavity. (b) Schematic of the two-photon nonresonant Stokes scattering between two vibrational states of the molecule ( $n = 0 \rightarrow 1$ ) mediated by a virtual state  $|v\rangle$ . A harmonic potential (solid lines) approximates the energy landscape of the ground electronic level (dashed lines). (c) Typical plasmonic cavity mode centered at the frequency  $\omega_c$  in the visible range, with the width associated with the decay rate  $\kappa$  related to  $\omega_c$  through the quality factor  $Q = \omega_c/\kappa$ .

strong Ohmic losses—that is, they are characterized by very low quality factors (typically  $Q \lesssim 10$ )—placing these systems deep in the *bad cavity* regime (see the sketch of a plasmon mode in Figure 1c). This system was recently addressed using a linearization scheme based on the classical Langevin equation for the displacements of plasmon and phonon fields.<sup>25</sup>

In this work, we complement this approach by employing an exact numerical solution of the quantum mechanical dynamics of the nonresonant Raman scattering process in a plasmonic cavity that fully describes the buildup of incoherent population of vibrations in the molecule, addressing the effect of phonon stimulated Stokes scattering, and furthermore, allows to account for the quantum and classical covariances between the two bosonic fields. This formalism thus predicts a variety of nonlinear quantum effects in the scattered signal that might have already been revealed in different Raman measurements, and opens the door for specific design of experimental configurations that can test, and eventually control, the underlying coherences within SERS.

## RESULTS AND DISCUSSION

**Theoretical Framework.** The interaction between plasmons and vibrations that governs the dynamics of a SERS process can be properly addressed by establishing the Hamiltonian of the system. To derive this Hamiltonian, let us consider the vibrational states of the ground electronic state of the molecule. In a simplified one-dimensional model the potential landscape of this state can be approximated as a displaced harmonic potential. Therefore, the vibrational levels separated by phonon frequency  $\omega_m$ <sup>26</sup> can be quantized using the creation and annihilation operators  $\hat{b}$  and  $\hat{b}^\dagger$ . We can thus define a linear polarizability of the molecule along this coordinate as  $\hat{\alpha}_v = R_v Q_v^0 (\hat{b} + \hat{b}^\dagger)$ ,<sup>1</sup> where  $R_v$  is the element of the Raman tensor and  $Q_v^0$  is the zero-point amplitude of the vibrations. The molecule is coupled to the quantized field of the cavity mode with resonant frequency  $\omega_c$  and effective volume

$V_{\text{eff}}$  which can be expressed by the plasmon annihilation ( $\hat{a}$ ) and creation ( $\hat{a}^\dagger$ ) operators as  $\hat{E} = i\sqrt{\frac{\hbar\omega_c}{2\epsilon V_{\text{eff}}}}(\hat{a} - \hat{a}^\dagger)$ , where  $\epsilon$  is the permittivity of the medium. Thus, the induced Raman dipole  $\hat{p}_R = \hat{\alpha}_v \hat{E}$  will be interacting with the cavity field  $\hat{E}$ , yielding the interaction Hamiltonian  $\hat{H}_I = -\hat{p}_R \hat{E}$ , which, after dropping the fast rotating terms  $\propto (\hat{a}^\dagger)^2$  and  $(\hat{a})^2$ , and redefining the equilibrium position of the vibrations, yields the nonlinear interaction Hamiltonian ( $\hbar = 1$ ):  $\hat{H}_I = -g\hat{a}^\dagger \hat{a} (\hat{b}^\dagger + \hat{b})$ , with the coupling coefficient  $g = R_v Q_v^0 \omega_c / (\epsilon V_{\text{eff}})$ . This definition can be related to the resonant emitter-plasmon coupling parameter of the Jaynes–Cummings Hamiltonian  $g_C$  and the Purcell factor  $F_P \propto Q/V_{\text{eff}}$  (see the discussion in Supporting Information). Interestingly, the interaction Hamiltonian  $\hat{H}_I$  is identical to the one used in optomechanical systems, in which the quantized oscillations of a cavity mirror modify the resonance frequency of the cavity.<sup>24,25</sup>

It should be noted that this approach is limited to the *off-resonant Raman scattering*, for which the virtual state mediating the Raman transition (Figure 1b) is strongly detuned from an excited electronic state. Also, our Hamiltonian does not consider Raman processes that involve the effect of the simultaneous excitation or emission of two or more phonons, which may become important for very intense lasers. Furthermore, our model assumes that the plasmonic system can be approximated as a single cavity mode, and described through the canonical quantization scheme. Although this approach should yield an accurate description for many of the plasmonic SERS setups, a more exact description could be offered by a rigorous quantization method which takes into account the exact Green's function of the system<sup>27,28</sup> and would allow consideration of complex plasmonic responses involving many modes.

The coherent evolution of the system, including an additional driving term (laser) at frequency  $\omega_l$  is then given by the full Hamiltonian

$$\hat{H} = \omega_m \hat{b}^\dagger \hat{b} + \omega_c \hat{a}^\dagger \hat{a} - g \hat{a}^\dagger \hat{a} (\hat{b}^\dagger + \hat{b}) + i\Omega (\hat{a}^\dagger e^{-i\omega_l t} - \hat{a} e^{i\omega_l t}) \quad (1)$$

Throughout the paper  $\Omega^2$  will be referred to as a *pumping power* proportional to the power density of the input laser and the intrinsic parameters of the cavity mode (see the discussion in Supporting Information).

The master equation for the dynamics of the density matrix of the system  $\rho$  in the absence of pure dephasing<sup>29</sup> reads

$$\partial_t \rho = i[\rho, \hat{H}] + \frac{\kappa}{2} \mathcal{D}_{\hat{a}}[\rho] + \frac{(n_b^{\text{th}} + 1)\gamma_m}{2} \mathcal{D}_{\hat{b}}[\rho] + \frac{n_b^{\text{th}} \gamma_m}{2} \mathcal{D}_{\hat{b}^\dagger}[\rho] \quad (2)$$

where the last three terms on the right-hand side are Lindblad–Kossakowski terms defined as<sup>30,31</sup>  $\mathcal{D}_{\hat{O}}[\rho] = 2\hat{O}\rho\hat{O}^\dagger - \hat{O}^\dagger\hat{O}\rho - \rho\hat{O}^\dagger\hat{O}$  describing the decay of the plasmons ( $\mathcal{D}_{\hat{a}}$ ), phonons ( $\mathcal{D}_{\hat{b}}$ ), and the thermal pumping ( $\mathcal{D}_{\hat{b}^\dagger}$ ) of the phonons by the environment at temperature  $T$ , with the thermal population  $n_b^{\text{th}} = (e^{\hbar\omega_m/k_B T} - 1)^{-1}$ .

In the following, we take the phonon energy  $\omega_m = 0.1$  eV and the phonon decay rate  $\gamma_m = 1$  meV,<sup>29</sup> as representative values that characterize vibrational fingerprints, and consider a typical plasmonic cavity with quality factor of  $Q = 10$  resonant at  $\omega_c =$

2.5 eV, decaying with rate  $\kappa = 0.25$  eV (see Supporting Information). The coupling parameter is taken as  $g = 1$  meV in accordance with the characteristics of state-of-the-art resonant plasmon-emitter systems (see Supporting Information).

To analyze the dynamics of the system, we follow three complementary approaches. First, we solve directly the master equation in eq 2 by means of numerical calculations,<sup>32</sup> (taking advantage of low excitation numbers to truncate the Hilbert space). We complement this numerical solution by two other approximate treatments that allow to obtain analytical results, useful to identify the influence of the different parameters in the Raman signal and thus provide simpler expressions to interpret experimental results. In the first analytical approximation, we linearize the Hamiltonian to a purely quadratic form which applies to the weak coupling ( $g \ll \kappa$ ) regime we are interested in, and allows for the analytical treatment (see Supporting Information for details). We note that when solving the linearized Hamiltonian, we do not map the quantum Langevin equation to the classical dynamics equations, as is often done in the analysis of optomechanical systems.<sup>24</sup> Consequently, this approach provides a complete characterization of the classical and quantum correlations within the system. Finally, to develop the second analytical approach, we apply the *quantum noise approach*,<sup>33</sup> in which the vibrations of the molecule are coupled to a bath of fluctuating population of the cavity plasmons.<sup>25</sup> This last formalism allows us to describe the effects of the *static* and *dynamical backaction*, which arise when the vibrations of the molecule modify the resonant frequency of the cavity and, therefore, the population term in the Hamiltonian (eq 1).<sup>24,34</sup> The static backaction describes the constant, coherent displacement of the state of the vibrations and can be largely neglected in the regime of parameters of interest (see the Methods section for a further discussion). On the other hand, the dynamical backaction (DBA), observed when the incident laser is detuned from the cavity, leads to the heating or cooling of the vibrations.<sup>24</sup> The quantum noise approach captures those effects, at the price of losing the information about coherences in the molecule-plasmon system.<sup>24,34</sup> The spectra of emission from the cavity are calculated following Glauber's photo-detection theory,<sup>35</sup> as  $I(\omega) = \alpha_{\text{det}} S(\omega)$ , where the frequency-independent parameter  $\alpha_{\text{det}}$  describes the properties of the detection system<sup>22</sup> and  $S(\omega) = \omega^4 \int_{-\infty}^{\infty} e^{-i\omega t} \langle \hat{a}^\dagger(t) \hat{a}(0) \rangle_{\text{ss}} dt$  in the steady state (ss). The two-time correlator is calculated by applying the *quantum regression theorem* (QRT).<sup>36</sup>

Let us first focus on the numerical solution. Two spectra of emission from the cavity, calculated for the weak ( $\Omega^2 = 10^{-2}$  eV<sup>2</sup>) and strong illuminations ( $\Omega^2 = 0.5$  eV<sup>2</sup>) and for the laser tuned to the cavity ( $\Delta \equiv \omega_c - \omega_l = 0$ ), are shown in Figure 2a and b, respectively. In the inset of Figure 2a we zoom in on the anti-Stokes emission calculated for the environment at  $T = 0$  K (dashed line) and  $T = 300$  K (solid line;  $n_b^{\text{th}}(T = 300 \text{ K}) \approx 0.02$ ). The difference between these plots illustrates the effect of *thermal pumping* of the vibrational levels by the environment.<sup>37,38</sup>

To further explore how the signal evolves with the pumping power, we plot in Figure 2c the maxima of the Stokes (blue solid line; in the region of interest this function is independent of the temperature  $T$ ) and anti-Stokes (orange dashed line for  $T = 0$  K and orange solid line for  $T = 300$  K) emission lines for an increasing  $\Omega^2$ . In the weak pumping regime ( $\Omega^2 \lesssim 10^{-2}$  eV<sup>2</sup>) for nonzero temperature (solid lines) both the Stokes  $S(\omega_s)$  and anti-Stokes  $S(\omega_{\text{as}})$  emission depend linearly on  $\Omega^2$ , indicating that the anti-Stokes transition originates from the

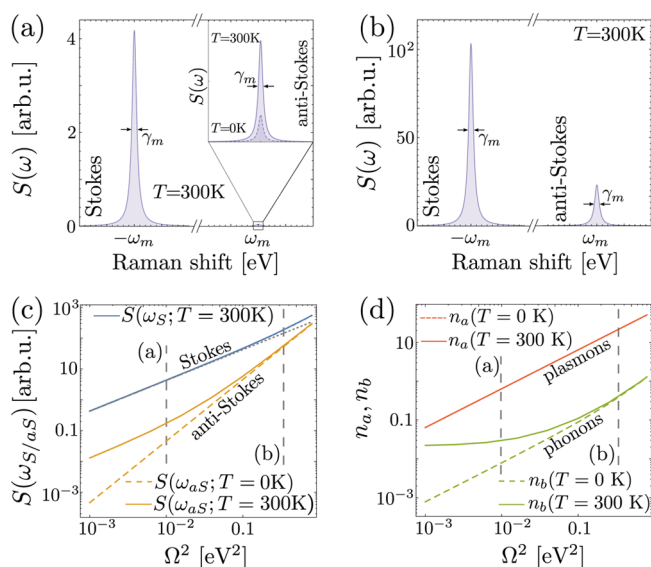


**Figure 2.** Dependence of the Raman scattering on the excitation power and temperature: (a,b) emission spectra  $S(\omega)$  of the molecule in the plasmonic cavity for pumping (a)  $\Omega^2 = 10^{-2}$  eV<sup>2</sup> and (b)  $\Omega^2 = 0.5$  eV<sup>2</sup> at  $T = 0$  K (dashed lines) and  $T = 300$  K (solid lines); (c) emission intensities of the Stokes ( $S(\omega_s)$ , blue lines, calculated at  $T = 300$  K) and anti-Stokes photons ( $S(\omega_{\text{as}})$ , orange dashed and solid lines for  $T = 0$  K and  $T = 300$  K, respectively) as a function of the pumping power  $\Omega^2$ ; (d) populations of plasmons (red line) and phonons (green lines) in the steady state for  $T = 0$  K (dashed lines) or  $T = 300$  K (solid lines). Vertical dashed lines in (c,d) indicate the pumping powers for plots in (a) and (b). All the cases assume  $\Delta = 0$ .

thermally excited vibrational state. For higher driving powers ( $10^{-2}$  eV<sup>2</sup>  $\lesssim \Omega^2 \lesssim 0.5$  eV<sup>2</sup>) the anti-Stokes intensities become independent of the temperature, as the phonons are provided primarily by the Stokes transitions (*vibrational pumping*).<sup>38</sup> The transition between the thermal and the vibrational pumping of phonons<sup>38</sup> is illustrated in Figure 2d, where we plot the populations of the phonons (green line) and plasmons (red line) for  $T = 0$  K (dashed lines) and  $T = 300$  K (solid lines).

Finally, for the highest considered pumping powers ( $\Omega^2 \gtrsim 0.5$  eV<sup>2</sup>) the Stokes intensity  $S(\omega_s)$  visibly surpasses the expected linear dependence on  $\Omega^2$  (marked with dotted gray line in the top-right corner of Figure 2c). To address this effect, we develop the first of the aforementioned analytical approaches by considering the linearized Hamiltonian and employing the QRT, which for the particular case of  $\Delta = 0$ ,  $\gamma_m \ll \omega_m$ ,  $\kappa$ , and environment temperature  $T$  yields the following expressions for the Stokes and anti-Stokes photons

$$S(\omega_s) = \frac{4\omega_s^4}{\gamma_m} s_2 \Omega^2 \left( 1 + n_b^{\text{th}} + s_2 \Omega^2 \frac{\kappa}{\gamma_m} \right) \quad (3)$$

and

$$S(\omega_{\text{as}}) = \frac{4\omega_{\text{as}}^4}{\gamma_m} s_2 \Omega^2 \left( n_b^{\text{th}} + s_2 \Omega^2 \frac{\kappa}{\gamma_m} \right) \quad (4)$$

with  $s_2 \approx [4g/(\kappa|k - 2i\omega_m|)]^2$  (see Supporting Information for the complete derivation). The first term in the brackets of eq 3 can be recognized as the conventional two-photon cavity-assisted Stokes transition, linearly dependent on  $\Omega^2$ . As we show in the Supporting Information, by considering the

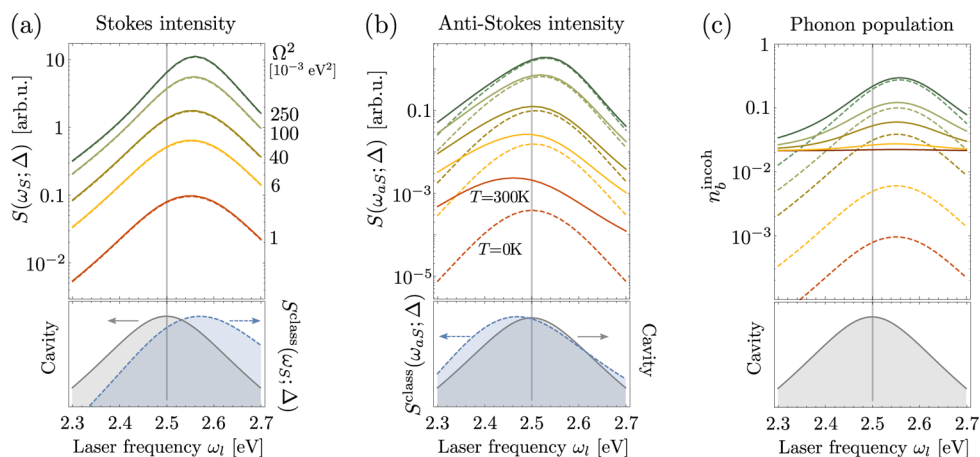


**Figure 3.** Dependence of the (a) Stokes and (b) anti-Stokes emission and (c) phonon population on the frequency of the incident laser  $\omega_l$ . In the two left-most top panels, we show the numerically calculated intensities (a) at the Stokes  $S(\omega_S; \Delta = \omega_c - \omega_l)$  and (b) at the anti-Stokes  $S(\omega_{AS}; \Delta)$  frequencies for the pumping power from  $\Omega^2 = 10^{-3} \text{ eV}^2$  (red lines) to  $\Omega^2 = 0.25 \text{ eV}^2$  (green lines) and environment temperature  $T = 0 \text{ K}$  (dashed lines) and  $T = 300 \text{ K}$  (solid lines). In bottom panels in (a, b) the dashed blue lines show the predictions of classical models (eq 5) for (a)  $S^{\text{class}}(\omega_S; \Delta)$  and (b)  $S^{\text{class}}(\omega_{AS}; \Delta)$ , whereas the cavity resonances are shown in (a–c) in gray. In (c), we plot the incoherent phonon population  $n_b^{\text{incoh}}$  calculated within the quantum noise approach eq 14. Identical results are obtained with the exact numerical calculation. The temperature and intensity for each situation are denoted with the same color code as in (a) and (b).

enhancement  $K = |E/E_0|$  of the electric component of the incident illumination  $E_0$  produced by the plasmonic cavity and relating it through the reciprocity theorem to the Purcell factor of the cavity,<sup>39,40</sup> this term in eq 3 allows us to retrieve the expected dependence of the Stokes emission  $S(\omega_S) \propto K^4$ .

The sum of the second and the third terms in brackets in eq 3, or the two terms in brackets in eq 4, represents the incoherent population of the phonon mode ( $n_b^{\text{incoh}} = \langle \hat{b}^\dagger \hat{b} \rangle_{ss} - \langle \hat{b}^\dagger \rangle_{ss} \langle \hat{b} \rangle_{ss}$ ) arising from (i) the thermal pumping and (ii) the coupling to the plasmon cavity, respectively. These two terms together describe a process of *phonon-stimulated Raman scattering*, in which the population of vibrations enhances the rate of Stokes scattering. Therefore, the last term in eq 3 explains the nonlinearity of the Stokes signal for large  $\Omega^2$ . We note that phonon-stimulated Raman scattering has been reported in experiments on ensembles of Raman-active centers, for example, hydrogen gas (see refs 41 and 42 and references therein). However, to our knowledge, the criterion for the onset of this effect for single scatterers in a cavity (see the Supporting Information for an explicit formulation) has not been reported in the literature.

To further explore the effects of the thermal and vibrational pumping of phonons on Raman scattering, we consider the dependence of the Raman scattering on the detuning  $\Delta = \omega_c - \omega_l$  of the incident laser. In the typical classical models of SERS,<sup>43</sup> the dependence of the Stokes ( $S^{\text{class}}(\omega_S; \Delta)$ ) and the anti-Stokes ( $S^{\text{class}}(\omega_{AS}; \Delta)$ ) emission is determined by the enhancement of the electric field of both the incoming ( $|E(\omega_l)/E_0(\omega_l)|^2$ ) and outgoing ( $|E(\omega_{S/AS})/E_0(\omega_{S/AS})|^2$ ) photons at the position of the molecule

$$S^{\text{class}}(\omega_{S/AS}; \Delta) \propto \omega_{S/AS}^4 \left| \frac{E(\omega_l)}{E_0(\omega_l)} \frac{E(\omega_{S/AS})}{E_0(\omega_{S/AS})} \right|^2 \quad (5)$$

Assuming that the enhancement is given by a Lorentzian profile centered on the cavity resonance  $\omega_c$  with width  $\kappa$  (gray curves in the bottom panels of Figure 3), we expect that the calculated Raman emission spectra  $S(\omega_{S/AS}; \Delta)$  will depend on the laser frequency as depicted with the blue dashed curves in the

bottom panels of Figure 3. In particular, the Stokes signal should be strongest for the incident laser blue-tuned from the cavity. This general result for the Stokes scattering is confirmed by our numerical calculations performed for various pumping powers ( $\Omega^2 = 10^{-3} \text{ eV}^2$  to  $0.25 \text{ eV}^2$ , from red to green lines) and different temperatures ( $T = 0 \text{ K}$  as dashed lines and  $300 \text{ K}$  as solid lines), as shown in the upper panels of Figure 3a.

However, there are also marked differences: we note that when the laser is blue-detuned from the cavity resonances ( $\Delta < 0$ ), the profile  $S(\omega_S; \Delta)$  becomes narrower as we increase the pumping intensity. This behavior results from the buildup of the incoherent population of phonons due to the vibrational pumping and to the dynamical backaction.<sup>34</sup> The latter phenomenon, triggered only when the laser is blue-detuned from the cavity resonance ( $\Delta < 0$ ), has been observed in optomechanical systems<sup>24</sup> and was recently argued to occur in Raman scattering from molecules.<sup>25</sup> We discuss this concept in more detail in the following paragraphs.

Interestingly, the classical eq 5 fails to explain the dependence of the anti-Stokes scattering obtained in the full quantum calculations (Figure 3b). For the weakest driving powers (red lines,  $\Omega^2 = 10^{-3} \text{ eV}^2$ ), the  $S(\omega_{AS}; \Delta)$  intensity is found to be the largest for the laser frequency  $\omega_l$  on resonance with the cavity  $\omega_c$  in the absence of thermal pumping of phonons ( $T = 0$ ); however this maximum appears as red-tuned from the cavity resonance when the thermal pumping of phonons is produced (at  $T = 300 \text{ K}$ ). For stronger driving powers, the intensity plots for  $T = 0$  and  $300 \text{ K}$  start to merge and peak at increasingly blue-shifted frequencies, notably crossing the cavity resonance. As for the supra-linear increase of the Stokes scattering, this surprising property stems from the laser pumping of the vibrational levels. The classical eq 5 for the anti-Stokes  $S^{\text{class}}(\omega_{AS}; \Delta)$  intensity does not account for the origin of the vibrations of the molecule and, therefore, can only be applied when these are provided by the heated reservoir (it should be noted, however, that a suitable correction to  $S(\omega_{AS}; \Delta)$  introducing the vibrational pumping has been proposed by Kneipp et al.<sup>37</sup>).

To understand the dependencies of the Stokes and anti-Stokes emission on the detuning presented in Figure 3a and b, we need to consider the vibrational state of the molecule in detail. Since the linearized Hamiltonian cannot be easily solved analytically for an arbitrary detuning  $\Delta$ , we develop an alternative analysis of the dynamics of the system based on the quantum noise approach,<sup>24,34</sup> which also allows to obtain analytical expressions for the Stokes and anti-Stokes photon emission. According to this approach, and similarly to the weak coupling model of a two-level system in a cavity, the rates of relaxation and excitation of vibrations are considered to be proportional to the noise spectrum determined by the characteristics of the plasmonic cavity. This coupling effectively modifies the decay rate of the molecular vibrations to  $\gamma_m + \gamma_{\text{opt}}$ , where the *optomechanical damping*  $\gamma_{\text{opt}}$  is dependent on the detuning  $\Delta$  and the intensity of the incident laser (see eq 15). Furthermore,  $\gamma_{\text{opt}}$  describes the exchange of energy between the vibrations and fluctuations of the cavity population about its mean value. A description of the quantum noise approach with the explicit expression of  $\gamma_{\text{opt}}$  [eq 15] is given in the Methods section. As a result, the intensities of the Stokes and anti-Stokes emissions for general detuning are given within the quantum noise approach by

$$S(\omega_s) \propto \frac{\omega_s^4 g^2 n_a^{\text{coh}} \kappa}{(\Delta + \omega_m)^2 + (\kappa/2)^2} \frac{n_b^{\text{incoh}} + 1}{\gamma_{\text{opt}} + \gamma_m} \quad (6)$$

and

$$S(\omega_{\text{as}}) \propto \frac{\omega_{\text{as}}^4 g^2 n_a^{\text{coh}} \kappa}{(\Delta - \omega_m)^2 + (\kappa/2)^2} \frac{n_b^{\text{incoh}}}{\gamma_{\text{opt}} + \gamma_m} \quad (7)$$

respectively, where  $n_b^{\text{incoh}}$  denotes the incoherent phonon population, and  $n_a^{\text{coh}}$  is the coherent population of the cavity (see the Methods section for the exact definition of these parameters). The dependence of  $n_b^{\text{incoh}}$  as a function of detuning and laser intensity, shown in Figure 3c and obtained from application of eq 14, helps to understand the dependences of the Stokes and anti-Stokes emission in Figure 3a and b. These analytical results are indeed identical to those obtained with the exact numerical solution.

For the laser blue-tuned from the plasmonic cavity ( $\Delta < 0$ ), the optomechanical damping  $\gamma_{\text{opt}}$  becomes negative, resulting in an increase of the incoherent phonon population  $n_b^{\text{incoh}}$ , as observed in Figure 3c. Consequently, the Stokes and anti-Stokes emission reveal similar dependence on  $\Delta$ , as shown in

$$g_{\Gamma_1, \Gamma_2}^{(2)}(\omega_1, \omega_2; \tau) = \lim_{t \rightarrow \infty} \frac{\langle : \mathcal{T} [\hat{A}_{\omega_1, \Gamma_1}^\dagger(t) \hat{A}_{\omega_2, \Gamma_2}^\dagger(t + \tau) \hat{A}_{\omega_2, \Gamma_2}(t + \tau) \hat{A}_{\omega_1, \Gamma_1}(t)] : \rangle}{\langle (\hat{A}_{\omega_1, \Gamma_1}^\dagger \hat{A}_{\omega_1, \Gamma_1})(t) \rangle \langle (\hat{A}_{\omega_2, \Gamma_2}^\dagger \hat{A}_{\omega_2, \Gamma_2})(t + \tau) \rangle} \quad (8)$$

where  $\mathcal{T}$  and “:” denote the time and normal ordering operators, respectively.<sup>47,48</sup> Furthermore,  $\hat{A}_{\omega, \Gamma}(t) = \int_{-\infty}^t e^{i(\omega - \Gamma/2)(t-t_1)} \hat{a}(t_1) dt_1$  is the field detected at frequency  $\omega$ , within a frequency window  $\Gamma$ , at time  $t$ . For simplicity we consider  $\Gamma_1 = \Gamma_2 = \Gamma$  and place the Lorentzian filters at  $\omega_{1/2} = \omega_{s/as}$ . The photon correlations  $g_{\Gamma, \Gamma}^{(2)}(\omega_s, \omega_{\text{as}}; \tau = 0)$ , calculated using a recently developed method,<sup>49</sup> are plotted in Figure 4a as a function of the driving parameter  $\Omega^2$  for an environment temperature of  $T = 0$  K (dashed lines) and  $T = 300$  K (solid lines). The details of the method of calculation of the correlation function are provided

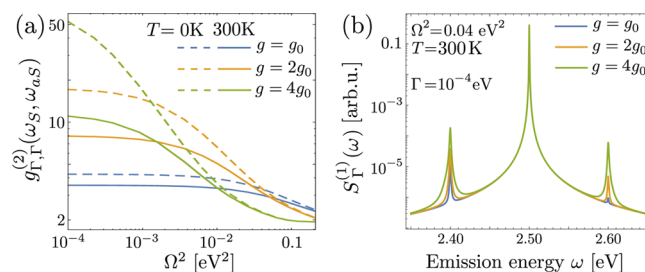


**Figure 4.** (a) Two-photon frequency-resolved Stokes-anti-Stokes correlators  $g_{\Gamma, \Gamma}^{(2)}(\omega_s, \omega_{\text{as}})$  and (b) physical spectra of emission  $S_{\Gamma}^{(1)}(\omega) = \langle \hat{A}_{\omega, \Gamma}^\dagger(0) \hat{A}_{\omega, \Gamma}(0) \rangle$  calculated for the temperatures  $T = 0$  K (dashed lines) and  $T = 300$  K (solid lines), coupling parameters chosen as multiples of  $g_0 = \kappa/250$ :  $g = g_0$  (blue lines),  $g = 2g_0$  (orange lines),  $g = 4g_0$  (green lines), and laser tuned to the cavity  $\Delta = 0$ .

Figure 3a and b. The Stokes and anti-Stokes peaks' widths exhibit also a narrowing from  $\gamma_m$  to  $\gamma_m + \gamma_{\text{opt}}$  which, interestingly, is compensated for by the denominators in the above equations, ensuring that the integrated intensity of the inelastic scattering is only implicitly dependent on  $\gamma_{\text{opt}}$  through  $n_b^{\text{incoh}}$ . Furthermore, we note that in analogy to other optomechanical systems, we can define a *cooperativity-like parameter*  $\tilde{C} = \gamma_{\text{opt}}/\gamma_m$  of the Raman process. For the parameters discussed throughout this work and for blue-tuned laser,  $\tilde{C}$  reaches the minimum value of  $-0.15$  for  $\Delta \approx -0.8\omega_m$  (see Figure S2 in the Supporting Information). For  $\tilde{C} \leq -1$  (in the case of laser blue-tuned from the cavity  $\Delta < 0$ ), the system would exhibit phonon lasing.<sup>25</sup>

On the other hand, for red-tuned laser ( $\Delta > 0$ ) we enter the so-called *cooling regime* in optomechanics, in which the vibrations can be suppressed below the thermal population  $n_b^{\text{th}}$ . However, because we are not in the sideband-resolved limit ( $\kappa \ll \omega_m$ ), in a typical SERS configuration this effect is suppressed, and  $n_b^{\text{incoh}}$  does not significantly drop below  $n_b^{\text{th}}$ , as illustrated by the solid lines in Figure 3c.

Last, we focus on an important piece of information regarding the characterization of Raman photon emission that can be obtained from the time- and frequency-resolved correlation<sup>44–46</sup> between Stokes and anti-Stokes photons emitted from the cavity. In the steady state, this magnitude can be theoretically calculated through intensity–intensity correlations of the filtered output field,

in Supporting Information. The coupling parameters  $g$  are considered as multiples of  $g_0 = \kappa/250$ , namely  $g = g_0$  (blue lines),  $g = 2g_0$  (orange lines),  $g = 4g_0$  (green lines), with the filter line width  $\Gamma = 0.1$  meV. As shown in Figure 4b, for these parameters the physical spectrum of emission  $S_{\Gamma}^{(1)}(\omega) = \langle \hat{A}_{\omega, \Gamma}^\dagger(0) \hat{A}_{\omega, \Gamma}(0) \rangle$  is formed by three peaks: the elastic Rayleigh scattering and inelastic Stokes and anti-Stokes contributions (note that  $S_{\Gamma}^{(1)}$  does not include the explicit dependence on the  $\omega^4$  factor). We clearly observe in Figure 4a that for weak coherent pumping and in the absence of thermal pumping (dashed lines), the system exhibits strong bunching statistics,

which is a signature of strongly correlated emission.<sup>50,51</sup> The physical origin of the strong correlation is discussed in detail in the [Supporting Information](#). In short, in the absence of other sources of excitations, the Raman photons are emitted by exchanging a single phonon and are therefore strongly correlated. This process should exhibit a  $g_{\text{r.f.}}^{(2)}(\omega_s, \omega_{\text{aS}}) \propto 1/S(\omega_s) \propto \Omega^{-2}$  dependence, as the rate of coincidences in the detection is determined by the anti-Stokes emission  $S(\omega_{\text{aS}})$ .<sup>52,53</sup> The results in [Figure 4a](#) show this evolution of the correlation for large incident power. As the thermal pumping (solid lines in [Figure 4a](#)) grows, the anti-Stokes photons are increasingly created through the absorption of phonons which originate from thermal excitation, leading to the quenching of the correlation. Finally, the dependence of the correlations on the coupling parameter stems from the fact that for small  $g$  (and weak anti-Stokes emission), the filters detect primarily the elastically scattered photons (see [Figure 4b](#)), leading to a plateau in  $g_{\text{r.f.}}^{(2)}(\omega_s, \omega_{\text{aS}})$  for small  $\Omega$ . We note that these results are consistent with those recently reported by Kasperczyk et al.<sup>52</sup> from measurements of the Stokes and anti-Stokes pairs emitted from a thin layer of diamond and by Parra-Murillo et al.<sup>53</sup> from the theoretical analysis of the Raman scattering.

## CONCLUSIONS

In summary, we have implemented a fully quantum-mechanical model of the inelastic nonresonant Raman scattering from a molecule placed in a lossy plasmonic cavity. Our analytical and exact numerical calculations point to phenomena which go beyond the standard description of Raman scattering such as (i) the onset of stimulated Stokes emission and (ii) the counterintuitive dependence of the anti-Stokes signal on the detuning of the incident laser from the cavity resulting from the pumping of the molecular vibrations. Furthermore, we demonstrate the strong correlations of Stokes and anti-Stokes pairs emitted from the cavity and analyze the origin of this effect. Finally, we note that our model can be readily applied to a range of physical problems, that is, investigating the Raman scattering of noncoherent light or the quantum correlations induced in the system.

## METHODS

**Linearization of the Optomechanical Hamiltonian.** Let us consider the optomechanical Hamiltonian given in [eq 1](#). If we decouple the cavity from the molecule (putting  $g = 0$ ), the plasmonic system is driven into a steady coherent state with amplitude  $\alpha_s = \Omega / (\frac{\kappa}{2} + i\Delta)$ . The interaction with these steady-state plasmons dominates the dynamics of the system in the weak-coupling regime as can be seen by the transformation to a displaced basis (with  $|\alpha_s\rangle \rightarrow |0\rangle$ ) in the plasmonic system. By, correspondingly, replacing  $\hat{a} \rightarrow \hat{a} + \alpha_s$ , we can express the coherent dynamics of the system through the Hamiltonian

$$\hat{H} = \Delta \hat{a}^\dagger \hat{a} + \omega_m \hat{b}^\dagger \hat{b} - g|\alpha_s|^2 (\hat{b} + \hat{b}^\dagger) - g(\alpha_s \hat{a}^\dagger + \alpha_s^* \hat{a}) (\hat{b} + \hat{b}^\dagger) - g \hat{a}^\dagger \hat{a} (\hat{b} + \hat{b}^\dagger) \quad (9)$$

As we discuss in the [Supporting Information](#) in detail, in the regime of parameters used throughout this work, characterized by weak coupling  $g$ , the last nonlinear term can be neglected, allowing us to write the simplified Hamiltonian

$$\hat{H}' = \Delta \hat{a}^\dagger \hat{a} + \omega_m \hat{b}^\dagger \hat{b} - g|\alpha_s|^2 (\hat{b} + \hat{b}^\dagger) - g(\alpha_s \hat{a}^\dagger + \alpha_s^* \hat{a}) (\hat{b} + \hat{b}^\dagger) \quad (10)$$

which yields a purely quadratic/Gaussian dynamics and linear quantum Langevin equations. We will refer to  $\hat{H}'$  as a *linearized Hamiltonian*.

In this new Hamiltonian, the coherent driving of the cavity gives rise (via the nonlinear interaction) to a linear coupling between phonons and plasmons (the last term in [eq 10](#)) and an effective coherent driving  $g|\alpha_s|^2$  of the phonon mode. To remove this driving term, we displace the phononic operators in the same way as for the plasmon and obtain a new coherent driving of the cavity (and a renormalized detuning), and so successively. We can capture *all* orders of this feedback by defining displacements  $\alpha'_s$  and  $\beta'_s$  through the condition that in the displaced basis the Hamiltonian does not contain any linear (*driving*) terms. Such displaced Hamiltonian can be written as

$$\hat{H}'' = \Delta' \hat{a}^\dagger \hat{a} + \omega_m \hat{b}^\dagger \hat{b} - g[\alpha'_s \hat{a}^\dagger + (\alpha'_s)^* \hat{a}] (\hat{b} + \hat{b}^\dagger) \quad (11)$$

where displacements  $\alpha'_s$  and  $\beta'_s$  are defined by

$$\alpha'_s = \frac{\Omega}{(\kappa/2) + i\Delta'} \quad (12)$$

$$\beta'_s = \frac{g|\alpha_s|^2}{\omega_m - i(\gamma_m/2)} \quad (13)$$

and the renormalized  $\Delta' = \Delta - 2g\text{Re}(\beta'_s)$ .

**Quantum Noise Approach.** In the quantum noise approach, the molecular vibrations are coupled to the plasmonic cavity described by the quantum noise density of the plasmon population fluctuations  $\hat{a}^\dagger \hat{a}$  defined as  $S_{\hat{F}\hat{F}}(\omega) = \int_{-\infty}^{\infty} e^{i\omega t} \langle \hat{F}(t) \hat{F}(0) \rangle dt$ , where  $\hat{F} = \hat{a}^\dagger \hat{a} - \langle \hat{a}^\dagger \hat{a} \rangle$  denotes the fluctuations of the plasmon number around the equilibrium, and the average is taken over the state of the uncoupled cavity ( $g = 0$ ). From  $S_{\hat{F}\hat{F}}$  we can obtain the effective relaxation and excitation rates of the vibrations. As a result, the molecular vibrations are in a displaced thermal state. The displacement is given by  $\beta'_s$ , and the incoherent population of the thermal state is

$$n_b^{\text{incoh}} = \frac{\gamma_m}{\gamma_m + \gamma_{\text{opt}}} n_b^{\text{th}} - \frac{\gamma_{\text{opt}}}{\gamma_m + \gamma_{\text{opt}}} n_{\text{rad}} \quad (14)$$

(see the previous section and the [Supporting Information](#) for details). The second term in [eq 14](#) describes the effective heating of the vibrations by the incoherent population of the cavity (associated with the fluctuations of its population) and dominates the population of phonons in the vibrational pumping regime. It should be noted that this important contribution to  $n_b^{\text{incoh}}$  cannot be derived by assuming a classical form of the cavity field.<sup>34,54</sup> The *optomechanical damping* is defined as

$$\gamma_{\text{opt}} = g^2 [S_{\hat{F}\hat{F}}(\omega_m) - S_{\hat{F}\hat{F}}(-\omega_m)] = g^2 n_a^{\text{coh}} \times \kappa \left\{ \frac{1}{(\Delta - \omega_m)^2 + (\kappa/2)^2} - \frac{1}{(\Delta + \omega_m)^2 + (\kappa/2)^2} \right\} \quad (15)$$

with  $n_a^{\text{coh}} = |\alpha_s|^2$  denoting the coherent population of the cavity. Here, we simplified the  $\hat{F}$  operator by considering the displaced cavity operators  $\hat{a} \rightarrow \hat{a} + \alpha'_s$  and dropping the quadratic term:  $\hat{F} \approx \sqrt{n_a^{\text{coh}}} (\hat{a} + \hat{a}^\dagger)$ .<sup>34</sup> The first (second) term in the brackets of [eq 15](#) corresponds to the transfer of energy from vibrations to the cavity (from the cavity to the vibrations). The more general form of  $\gamma_{\text{opt}}$  includes the *static displacement* of vibrations, which can be accounted for by replacing the detuning  $\Delta$  in [eq 15](#) by  $\Delta'$  defined earlier. However, in the regime of parameters of interest in a typical Raman configuration, this correction is negligible. The second term in [eq 14](#)—the contribution to the population of vibrations originating from the coupling to the optical cavity—is proportional to  $n_{\text{rad}}$  with

$$n_{\text{rad}} = -\frac{(\Delta - \omega_m')^2 + (\kappa/2)^2}{4\Delta\omega_m'} \quad (16)$$

Here,  $\omega'_m$  is the mechanical frequency corrected for the *optical spring effect*.<sup>24,34</sup> This correction, however, can be neglected for the parameters in the regime of interest in SERS.

Finally, we note that in the limit of laser tuned to the cavity resonance  $\Delta \rightarrow 0$ , there is no DBA mechanism and the optomechanical damping  $\gamma_{\text{opt}}$  vanishes. In this case, and neglecting the static displacement of vibrations ( $\Delta \approx \Delta'$ ), we reproduce within the quantum noise approach the simple expression for the vibrationally pumped incoherent population of vibrations derived earlier from the full quantum-mechanical linearized treatment, thus making both analytical derivations fully consistent

$$\lim_{\Delta \rightarrow 0} n_b^{\text{incoh}} = n_b^{\text{th}} + \frac{4g_0^2 n_a^{\text{coh}} \kappa}{\kappa^2 + 4\omega_m^2 \gamma_m} \approx n_b^{\text{th}} + s_2 \Omega^2 \frac{\kappa}{\gamma_m} \quad (17)$$

Similarly, the expressions for the photon emission intensities  $S(\omega_s)$  and  $S(\omega_{\text{as}})$  obtained in eqs 6 and 7 with application of the quantum noise approach, also match those obtained from the previous analytical derivation (eqs 3 and 4).

## ASSOCIATED CONTENT

### Supporting Information

The Supporting Information is available free of charge on the ACS Publications website at DOI: 10.1021/acsnano.6b02484.

Estimation of parameters  $g$  and  $\Omega$  of the system; analytical solution to the linearized Hamiltonian within QRT; description of the correlation measurements. (PDF)

## AUTHOR INFORMATION

### Corresponding Authors

\*E-mail: aizpurua@ehu.es.

\*E-mail: mikolaj\_schmidt@ehu.es.

### Notes

The authors declare no competing financial interest.

## ACKNOWLEDGMENTS

M.K.S., R.E., and J.A. acknowledge funding from the project FIS2013-41184-P of the Spanish Ministry of Economy and Competitiveness, the ETORTEK IE14-393 NANOGUNE'14 project of the Department of Industry of the Government of the Basque Country, project IT756-13 of the Department of Education and Culture of the Basque Country, scholarship AP-2012-4204 from the Spanish Ministry of Education, Culture and Sport, financial assistance award 70NANB15H32 from U.S. Department of Commerce, National Institute of Standards and Technology, and the Fellows Gipuzkoa program of the Gipuzkoako Foru Aldundia through the FEDER funding scheme of the European Union, Una manera de hacer Europa. A.G.T. acknowledges support from the IntraEuropean Fellowship NanoQuIS (625955).

## REFERENCES

- (1) Ru, E. C. L.; Etchegoin, P. G. *Principles of Surface-Enhanced Raman Spectroscopy*; Elsevier: Amsterdam, 2009.
- (2) Nie, S. M.; Emory, S. R. Probing Single Molecules and Single Nanoparticles by Surface Enhanced Raman Scattering. *Science* **1997**, *275*, 1102–1106.
- (3) Kneipp, K.; Wang, Y.; Kneipp, H.; Perelman, L. T.; Itzkan, I.; Dasari, R. R.; Feld, M. S. Single Molecule Detection Using Surface-Enhanced Raman Scattering (SERS). *Phys. Rev. Lett.* **1997**, *78*, 1667–1670.
- (4) Sharma, B.; Frontiera, R. R.; Henry, A.-I.; Ringe, E.; Van Duyne, R. P. SERS Materials, Applications, and the Future. *Mater. Today* **2012**, *15*, 16–25.

(5) Jackson, J. B.; Halas, N. J. Surface-Enhanced Raman Scattering on Tunable Plasmonic Nanoparticle Substrates. *Proc. Natl. Acad. Sci. U. S. A.* **2004**, *101*, 17930–17935.

(6) Li, J. F.; Huang, Y. F.; Ding, Y.; Yang, Z. L.; Li, S. B.; Zhou, X. S.; Fan, F. R.; Zhang, W.; Zhou, Z. Y.; Wu, D. Y.; Ren, B.; Wang, Z. L.; Tian, Z. Q. Shell-isolated Nanoparticle-Enhanced Raman Spectroscopy. *Nature* **2010**, *464*, 392–395.

(7) Banaee, M. G.; Crozier, K. B. Gold Nanorings as Substrates for Surface-Enhanced Raman Scattering. *Opt. Lett.* **2010**, *35*, 760–762.

(8) Sivapalan, S. T.; DeVetter, B. M.; Yang, T. K.; van Dijk, T.; Schulmerich, M. V.; Carney, P. S.; Bhargava, R.; Murphy, C. J. Off-Resonance Surface-Enhanced Raman Spectroscopy from Gold Nanorod Suspensions as a Function of Aspect Ratio: Not What We Thought. *ACS Nano* **2013**, *7*, 2099–2105.

(9) D'Andrea, C.; Bochterle, J.; Toma, A.; Huck, C.; Neubrech, F.; Messina, E.; Fazio, B.; Marago, O. M.; Fabrizio, E. D.; de La Chapelle, M. L.; Gucciardi, P. G.; Pucci, A. Optical Nanoantennas for Multiband Surface-Enhanced Infrared and Raman Spectroscopy. *ACS Nano* **2013**, *7*, 3522–3531.

(10) Niu, W.; Chua, Y. A. A.; Zhang, W.; Huang, H.; Lu, X. Highly Symmetric Gold Nanostars: Crystallographic Control and Surface-Enhanced Raman Scattering Property. *J. Am. Chem. Soc.* **2015**, *137*, 10460–10463.

(11) Xu, H. X.; Bjerneld, E. J.; Käll, M.; Borjesson, L. Spectroscopy of Single Hemoglobin Molecules by Surface Enhanced Raman Scattering. *Phys. Rev. Lett.* **1999**, *83*, 4357.

(12) Talley, C. E.; Jackson, J. B.; Oubre, C.; Grady, N. K.; Hollars, C. W.; Lane, S. M.; Huser, T. R.; Nordlander, P.; Halas, N. J. Surface-Enhanced Raman Scattering from Individual Au Nanoparticles and Nanoparticle Dimer Substrates. *Nano Lett.* **2005**, *5*, 1569–1574.

(13) Zhu, W.; Crozier, K. B. Quantum Mechanical Limit to Plasmonic Enhancement as Observed by Surface-Enhanced Raman Scattering. *Nat. Commun.* **2014**, *5*, 5228.

(14) Park, W.-H.; Ahn, S.-H.; Kim, Z. H. Surface-Enhanced Raman Scattering from a Single Nanoparticle-Plane. *ChemPhysChem* **2008**, *9*, 2491.

(15) Rodríguez-Lorenzo, L.; Álvarez-Puebla, R. A.; de Abajo, F. J. G.; Liz-Marzán, L. M. Surface Enhanced Raman Scattering Using Star-Shaped Gold Colloidal Nanoparticles. *J. Phys. Chem. C* **2010**, *114*, 7336–7340.

(16) Sonntag, M. D.; Pozzi, E. A.; Jiang, N.; Hersam, M. C.; Dwyne, R. P. V. Recent Advances in Tip-Enhanced Raman Spectroscopy. *J. Phys. Chem. Lett.* **2014**, *5*, 3125–3130.

(17) Lombardi, A.; Demetriadou, A.; Weller, L.; Andrae, P.; Benz, F.; Chikkaraddy, R.; Aizpurua, J.; Baumberg, J. J. Anomalous Spectral Shift of Near- and Far-Field Plasmonic Resonances in Nanogaps. *ACS Photonics* **2016**, *3*, 471–477.

(18) Ye, J.; Wen, F.; Sobhani, H.; Lassiter, J. B.; Dorpe, P. V.; Nordlander, P.; Halas, N. J. Plasmonic Nanoclusters: Near Field Properties of the Fano Resonance Interrogated with SERS. *Nano Lett.* **2012**, *12*, 1660–1667.

(19) Xu, H.; Aizpurua, J.; Käll, M.; Apell, P. Electromagnetic Contributions to Single-molecule Sensitivity in Surface-Enhanced Raman Scattering. *Phys. Rev. E: Stat. Phys., Plasmas, Fluids, Relat. Interdiscip. Top.* **2000**, *62*, 4318–4324.

(20) Zhang, R.; Zhang, Y.; Dong, Z.; Jiang, S.; Zhang, C.; Chen, L.; Zhang, L.; Liao, Y.; Aizpurua, J.; Luo, Y.; Yang, J.; Hou, J. Chemical Mapping of a Single Molecule by Plasmon-Enhanced Raman Scattering. *Nature* **2013**, *498*, 82–86.

(21) Shalabney, A.; George, J.; Hutchison, J.; Pupillo, G.; Genet, C.; Ebbesen, T. W. Coherent Coupling of Molecular Resonators with a Microcavity Mode. *Nat. Commun.* **2015**, *6*, 5981.

(22) Johansson, P.; Xu, H.; Käll, M. Surface-Enhanced Raman Scattering and Fluorescence near Metal Nanoparticles. *Phys. Rev. B: Condens. Matter Mater. Phys.* **2005**, *72*, 035427.

(23) Xu, H.; Wang, X.-H.; Persson, M. P.; Xu, H. Q.; Käll, M.; Johansson, P. Unified Treatment of Fluorescence and Raman Scattering Processes near Metal Surfaces. *Phys. Rev. Lett.* **2004**, *93*, 243002.

- (24) Aspelmeyer, M.; Kippenberg, T. J.; Marquardt, F. Cavity Optomechanics. *Rev. Mod. Phys.* **2014**, *86*, 1391–1452.
- (25) Roelli, P.; Galland, C.; Piro, N.; Kippenberg, T. J. Molecular Cavity Optomechanics: a Theory of Plasmon-Enhanced Raman Scattering. *Nat. Nanotechnol.* **2015**, *11*, 164–169.
- (26) Bougeard, D.; Smirnov, K. S. Calculation of Off-Resonance Raman Scattering Intensities with Parametric Models. *J. Raman Spectrosc.* **2009**, *40*, 1704–1719.
- (27) Scheel, S.; Buhmann, S. Y. Macroscopic Quantum Electrodynamics - Concepts and Applications. *Acta Phys. Slovaca* **2008**, *58*, 675–809.
- (28) Dung, H. T.; Buhmann, S. Y.; Knöll, L.; Welsch, D.-G.; Scheel, S.; Kästel, J. Electromagnetic-Field Quantization and Spontaneous Decay in Left-Handed Media. *Phys. Rev. A: At., Mol., Opt. Phys.* **2003**, *68*, 043816.
- (29) Yampolsky, S.; Fishman, D. A.; Dey, S.; Hulkko, E.; Banik, M.; Potma, E. O.; Apkarian, V. A. Seeing a Single Molecule Vibrate Through Time-resolved Coherent Anti-Stokes Raman Scattering. *Nat. Photonics* **2014**, *8*, 650–656.
- (30) Gorini, V.; Kossakowski, A.; Sudarshan, E. C. G. Completely Positive Dynamical Semigroups of N-level Systems. *J. Math. Phys.* **1976**, *17*, 821–825.
- (31) Lindblad, G. On the Generators of Quantum Dynamical Semigroups. *Commun. Math. Phys.* **1976**, *48*, 119–130.
- (32) Navarrete-Benlloch, C. Open Systems Dynamics: Simulating Master Equations in the Computer. 2015, *arXiv:1504.05266*. arXiv.org e-Print archive. <http://arxiv.org/abs/1504.05266> (accessed May 2016).
- (33) Clerk, A. A.; Devoret, M. H.; Girvin, S. M.; Marquardt, F.; Schoelkopf, R. J. Introduction to Quantum Noise, Measurement, and Amplification. *Rev. Mod. Phys.* **2010**, *82*, 1155–1208.
- (34) Aspelmeyer, M.; Kippenberg, T. J.; Marquardt, F. *Cavity Optomechanics: Nano-and Micromechanical Resonators Interacting with Light*; Springer: New York, 2014.
- (35) Glauber, R. J. Photon Correlations. *Phys. Rev. Lett.* **1963**, *10*, 84.
- (36) Carmichael, H. J. *Statistical Methods in Quantum Optics I: Master Equation and Fokker-Planck Equations*; Springer Science & Business Media: New York, 2002; Vol. 1.
- (37) Kneipp, K.; Wang, Y.; Kneipp, H.; Itzkan, I.; Dasari, R. R.; Feld, M. S. Population Pumping of Excited Vibrational States by Spontaneous Surface-Enhanced Raman Scattering. *Phys. Rev. Lett.* **1996**, *76*, 2444–2447.
- (38) Maher, R.; Etchegoin, P.; Le Ru, E.; Cohen, L. A Conclusive Demonstration of Vibrational Pumping Under Surface Enhanced Raman Scattering Conditions. *J. Phys. Chem. B* **2006**, *110*, 11757–11760.
- (39) Carminati, R.; Nieto-Vesperinas, M.; Greffet, J.-J. Reciprocity of Evanescent Electromagnetic Waves. *J. Opt. Soc. Am. A* **1998**, *15*, 706–712.
- (40) Esteban, R.; Laroche, M.; Greffet, J.-J. Influence of Metallic Nanoparticles on Upconversion Processes. *J. Appl. Phys.* **2009**, *105*, 033107.
- (41) Wang, C.-S. Theory of Stimulated Raman Scattering. *Phys. Rev.* **1969**, *182*, 482–494.
- (42) Becker, P.; Bohaty, L.; Rhee, H.; Eichler, H. J.; Kaminskii, A. A.; Hanuza, J. Observation of Many-phonon Stimulated Raman Scattering and Related Cascaded Nonlinear-Laser Effects in Monoclinic LaBO<sub>2</sub> MoO<sub>4</sub> Single Crystals. *Laser Phys. Lett.* **2008**, *5*, 114.
- (43) Alonso-González, P.; Albella, P.; Schnell, M.; Chen, J.; Huth, F.; García-Etxarri, A.; Casanova, F.; Golmar, F.; Arzubiaga, L.; Hueso, L.; Aizpurua, J.; Hillenbrand, R. Resolving the Electromagnetic Mechanism of Surface-Enhanced Light Scattering at Single Hot Spots. *Nat. Commun.* **2012**, *3*, 684.
- (44) Cohen-Tannoudji, C.; Reynaud, S.; Bullough, R. K.; Vaughan, J. M. Atoms in Strong Light-Fields: Photon Antibunching in Single Atom Fluorescence. *Philos. Trans. R. Soc., A* **1979**, *293*, 223.
- (45) Silva, B.; González-Tudela, A.; Sánchez Muñoz, C.; Ballarini, D.; Gigli, G.; West, K. W.; Pfeiffer, L.; del Valle, E.; Sanvitto, D.; Laussy, F. P. Measuring Photon Correlations Simultaneously in Time and Frequency. 2014, *arXiv:1406.0964*. arXiv.org e-Print archive. <http://arxiv.org/abs/1406.0964> (accessed May 2016).
- (46) Hanbury Brown, R.; Twiss, R. Q. A Test of a New Type of Stellar Interferometer on Sirius. *Nature* **1956**, *178*, 1046.
- (47) Cresser, J. D. Intensity Correlations of Frequency-filtered Light Fields. *J. Phys. B: At. Mol. Phys.* **1987**, *20*, 4915.
- (48) Knöll, L.; Vogel, W.; Welsch, D.-G. Quantum Noise in Spectral Filtering of Light. *J. Opt. Soc. Am. B* **1986**, *3*, 1315–1318.
- (49) del Valle, E.; González-Tudela, A.; Laussy, F. P.; Tejedor, C.; Hartmann, M. J. Theory of Frequency-Filtered and Time-Resolved N-Photon Correlations. *Phys. Rev. Lett.* **2012**, *109*, 183601.
- (50) González-Tudela, A.; Laussy, F. P.; Tejedor, C.; Hartmann, M. J.; del Valle, E. Two-photon Spectra of Quantum Emitters. *New J. Phys.* **2013**, *15*, 033036.
- (51) del Valle, E. Distilling One, Two and Entangled Pairs of Photons from a Quantum Dot with Cavity QED Effects and Spectral Filtering. *New J. Phys.* **2013**, *15*, 025019.
- (52) Kasperczyk, M.; Jorio, A.; Neu, E.; Maletinsky, P.; Novotny, L. Stokes-anti-Stokes Correlations in Diamond. *Opt. Lett.* **2015**, *40*, 2393–2396.
- (53) Parra-Murillo, C. A.; Santos, M. F.; Monken, C. H.; Jorio, A. Stokes-anti-Stokes correlation in the inelastic scattering of light by matter and generalization of the Bose-Einstein population function. *Phys. Rev. B: Condens. Matter Mater. Phys.* **2016**, *93*, 125141.
- (54) Clerk, A. A.; Marquardt, F. *Cavity Optomechanics*; Springer: New York, 2014; pp 5–23.